Low-Temperature Toughening Mechanism in Thermomechanically Processed High-Strength Low-Alloy Steels

BYOUNGCHUL HWANG, CHANG GIL LEE, and SUNG-JOON KIM

High-strength low-alloy (HSLA) steels were fabricated by varying thermomechanical processing conditions such as rolling and cooling conditions in the intercritical region, and the low-temperature toughening mechanism was investigated in terms of microstructure and the associated grain boundary characteristics. The steels acceleratedly cooled to relatively higher temperature had lower tensile strength than those acceleratedly cooled to room temperature due to the increased volume fraction of granular bainite or polygonal ferrite (PF) irrespective of rolling in the intercritical region, while the yield strength was dependent on intercritical rolling, and start and finish cooling temperatures, which affected the formation of PF and low-temperature transformation phases. The steel rolled in the intercritical region and cooled to 673 K (400 °C) provided the best combination of high yield strength and excellent low-temperature toughness because of the presence of fine PF and appropriate mixture of various low-temperature transformation phases such as granular bainite, degenerate upper bainite (DUB), lower bainite (LB), and lath martensite (LM). Despite the high yield strength, the improvement of low-temperature toughness could be explained by the reduction of overall effective grain size based on the electron backscattered diffraction (EBSD) analysis data, leading to the decrease in ductile-to-brittle transition temperature (DBTT).

I. INTRODUCTION

HIGH-STRENGTH low-alloy (HSLA) steels widely used for building, bridge, pressure vessel, offshore, and pipeline structures have increasingly required higher strength, enhanced low-temperature toughness, and improved weldability simultaneously. In recent years, special attention has been paid to sufficient deformability such as low yield to tensile strength ratio, high uniform elongation, and high work hardening exponent, since many steel structures are subjected to progressive or abrupt displacement arising from structure loading itself, ground movement under their service environment, and earthquake.[1,2] As the increase of strength is often accompanied by the deterioration of toughness or deformability, a precise metallurgical design comprising chemical composition and thermomechanical processing is indispensible for achieving an excellent balance of the mechanical properties of HSLA steels. Presently, dual-phase microstructure is known to be very suitable for so-called *strain-based design* with higher deformability, because it offers superior strain capacity due to the initial yielding in soft ferrite phase and the subsequent strain hardening during load transfer to hard phase.[3–5]

In general, controlled rolling and cooling in the intercritical-phase region, *i.e.*, (austenite + ferrite) two-phase region, allow dispersion of stronger ferrite uniformly in the austenite, and subsequent accelerated cooling or quenching transforms the austenite to various low-temperature transformation phases depending on the cooling rate and start and finish cooling temperatures.[5–8] In dual-phase steels consisting of ferrite and low-temperature transformation phases, ferrite provides a beneficial effect for cleavage fracture resistance as well as good deformability, and the strength usually increases with the volume fraction of harder low-temperature transformation phases at the expense of toughness. However, recent progress in thermomechanical processing technology has shown that HSLA steels having higher strength and deformability can be efficiently fabricated without loss of toughness and weldability.[5,8] Because the morphologies of continuously cooled microstructures produced in low carbon or ultra-low-carbon HSLA steels have been regarded as very complicated,[9–11] on the other hand, systematic studies are seriously needed to elucidate the low-temperature toughening mechanism in terms of microstructure and the associated grain boundary characteristics.

In the present study, advanced thermomechanical processing conditions were employed to develop different dual-phase microstructures characterized by grain refinement and formation of various low-temperature transformation phases. Six kinds of HSLA steels were prepared by varying rolling and cooling conditions in the intercritical region, and then tensile and Charpy

BYOUNGCHUL HWANG, Senior Researcher, and CHANG GIL LEE, Principal Researcher, Ferrous Alloys Group, and SUNG-JOON KIM, Principal Researcher, are with the Korea Institute of Materials Science, Changwon 641-010, Korea. Contact e-mail: entropy0@kims.re.kr
Manuscript submitted April 24, 2010.
Article published online November 10, 2010.

impact tests were carried out on them to investigate the effect of intercritical rolling and cooling conditions on mechanical properties such as strength, deformability, and low-temperature toughness. The effective grain size and grain boundary characteristics were analyzed using electron backscattered diffraction (EBSD) analysis to interpret the low-temperature toughening mechanism from the standpoint of cleavage crack propagation.

II. EXPERIMENTAL

The nominal composition of steels investigated in the present study is Fe-0.07C-0.25Si-1.9Mn-0.5Ni-0.6Cr-0.25Mo-0.06Nb-0.03V-0.015Ti (wt pct). Table I provides detailed chemistry of six steel ingots. They were processed by varying conditions of rolling in the intercritical region and the subsequent cooling using laboratory-scale thermomechanical processing equipment, as shown in Figure 1 and Tables II and III. For convenience, they are referred to as SA, SB, SC, IA, IB, and IC steels, where the prefix letters S and I represent the steels rolled in the single- and intercritical-phase regions, respectively, and the subsequent letters A, B, and C refer to the different cooling conditions. After austenitization at 1423 K (1150 °C) for 2 hours, rolling was started at 1353 K (1080 °C) and finished at two temperatures, 1053 K and 993 K (780 °C and 720 °C), which were the temperature in the austenite single-phase region over Ar_3 and the temperature in the intercritical-phase region between Ar_3 and Ar_1, respectively. An overall grain refinement effect was expected by rolling with a high rolling reduction ratio above 70 pct in the nonrecrystallization region of austenite. After finish rolling, the steel was acceleratedly cooled at a rate above 10 °C/s to either 673 K (400 °C) or room temperature from 973 K or 873 K (700 °C or 600 °C) followed by air cooling (Figure 1). Because the initial and final thicknesses of steels were 100 and 12 mm, respectively, the total rolling reduction ratio was 88 pct.

Longitudinal-transverse (L-T) and longitudinal–short transverse (L-S) planes of the rolled steels were polished and etched by a 2 pct nital solution, and their
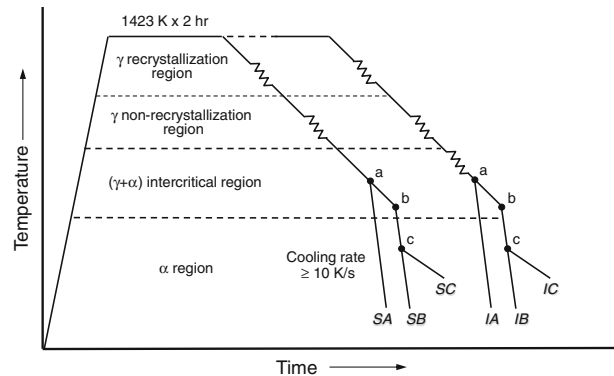

Fig. 1—Schematic illustration of thermomechanical processing conditions. *a* and *b* indicate the start cooling temperature of 973 K (700 °C) and 873 K (600 °C), respectively, and *c* the finish cooling temperature of 673 K (400 °C).

Table I. Chemical Compositions (Weight Percent)

	C	Si	Mn	Ni	Cr	Mo	Nb	V	Ti	Al	N*	B*	P*	S*
SA	0.070	0.25	1.89	0.49	0.59	0.25	0.063	0.026	0.015	0.016	56	11	60	15
SB	0.070	0.25	1.88	0.49	0.59	0.25	0.063	0.023	0.016	0.023	44	11	61	15
SC	0.071	0.25	1.89	0.49	0.59	0.25	0.064	0.026	0.017	0.026	47	11	62	14
IA	0.068	0.25	1.88	0.49	0.57	0.25	0.063	0.028	0.016	0.028	40	11	57	15
IB	0.071	0.25	1.90	0.49	0.60	0.25	0.063	0.027	0.017	0.027	45	12	57	14
IC	0.071	0.25	1.91	0.49	0.60	0.25	0.064	0.029	0.017	0.029	41	11	59	12

*Parts per million.

Table II. Rolling Schedules

	Steels Rolled in the Single-Phase Region			Steels Rolled in the Intercritical-Phase Region		
Pass	Thickness (mm)	Temperature K (°C)	Rolling Reduction (Pct)	Thickness (mm)	Temperature K (°C)	Rolling Reduction (Pct)
0	100	1423 (1150)	—	100	1423 (1150)	—
1	90	1353 (1080)	10.0	90	1353 (1080)	10.0
2	80	1333 (1060)	11.1	80	1333 (1060)	11.1
3	70	1313 (1040)	12.5	70	1313 (1040)	12.5
4	60	1293 (1020)	14.3	60	1293 (1020)	14.3
5	50	1273 (1000)	16.7	50	1273 (1000)	16.7
6	40	1123 (850)	20.0	40	1123 (850)	20.0
7	30	1103 (830)	25.0	30	1093 (820)	25.0
8	20	1083 (810)	33.3	20	1073 (800)	33.3
9	15	1068 (795)	25.0	15	1053 (780)	25.0
10	12	1053 (780)	20.0	13	1023 (750)	13.3
11	—	—	—	12	993 (720)	7.7

Table III. Thermomechanical Processing Conditions

Steel	SA	SB	SC	IA	IB	IC
Reheating temperature K (°C)	1423 (1150)					
Start Rolling temperature K (°C)	1353 (1080)					
Finish Rolling temperature K (°C)	1053 (780)			993 (720)		
Rolling reduction in Non-Recrystallization Region (Pct)	76			70		
Rolling reduction in intercritical Region (Pct)			—	20		
Start cooling temperature K (°C)	973 (700)	873 (600)	878 (605)	973 (700)	873 (600)	873 (600)
Finish cooling temperature K (°C)	RT*	RT*	748 (475)	RT*	RT*	693 (420)
Cooling rate K/s	12.2	16.9	16.3	10.4	14.8	18.0

*Room temperature.
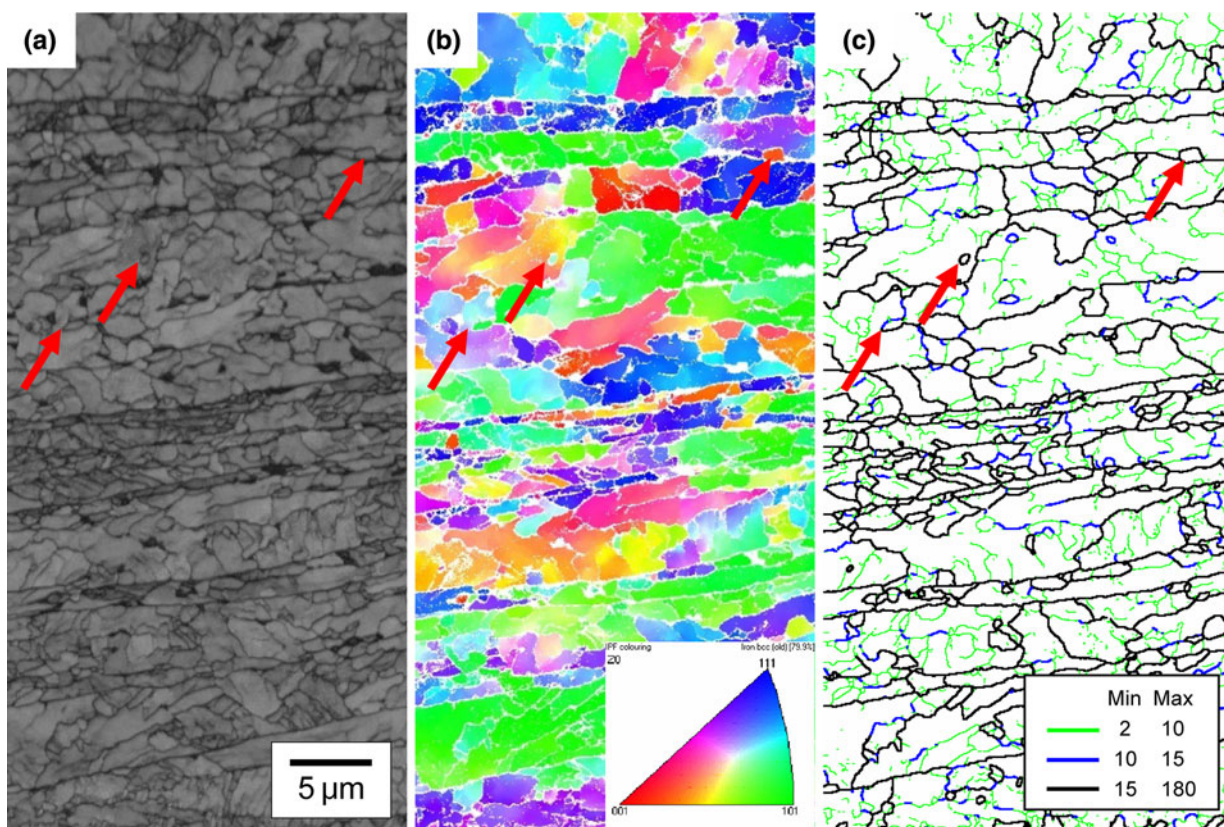
Fig. 2—EBSD analysis results showing microstructural features of PF as indicated by red arrows: (*a*) band contrast, (*b*) inverse pole figure, and (*c*) misorientation maps of the L-S plane of the SC steel. A stereographic triangle shows the correspondence between colors and crystal orientations.

microstructures were observed by an optical microscope and a field emission–scanning electron microscope (FE-SEM) (model JSM-7001F, JEOL*). In addition,

*JEOL is a trademark of Japan Electron Optics Ltd., Tokyo.

EBSD analysis was conducted on them to investigate the grain boundary characteristics of microstructures. The data were then interpreted by HKL Technology Channel 5 analysis software provided by Oxford Instruments, Inc. (Concord, MA). A more detailed metallographic examination was performed on the SC steel using a

transmission electron microscope (TEM) (model JEM-2100F, JEOL). After thin foils for TEM observations were prepared in a twin-jet electrolytic polishing apparatus using a solution containing 5 vol pct perchloric acid and 95 vol pct methanol, the microstructure was examined at 200 kV and the corresponding Kikuchi patterns were analyzed.

Figure 2 shows the band contrast, inverse pole figure, and misorientation maps obtained from EBSD analysis for the SC steel. In optical and SEM micrographs, polygonal ferrite (PF) is not readily identified because of some ambiguity due to its fine scale structure and distribution as compared to other phases. Although

TEM is a useful technique to estimate ferrite, many TEM micrographs should be taken to measure its volume fraction. In the present study, therefore, PF was defined as isolated and equiaxed fine domain with its relatively low band contrast and high-angle grain boundary in the EBSD maps as indicated by red arrows (Figure 2). The volume fraction of PF was measured by an image analyzer, and the other microstructures were identified according to their microhardness and morphologies.

Subsize round tensile test specimens with a gage diameter of 6.35 mm and a gage length of 25.4 mm were prepared in both transverse and longitudinal directions and tested at room temperature at a crosshead speed of 5 mm/min using a 10-ton universal testing machine (model INSTRON 5882**). The data reported in this

---

**INSTRON is a trademark of Instron Co., Norwood, MA.

---

study indicate an average of at least three tests. Charpy impact tests were performed in the temperature range of 77 K to 293 K (–196 °C to 20 °C) on standard Charpy V-notch specimens with a 10 × 10 × 55 mm size, which were machined in the transverse-longitudinal (T-L) orientation. A regression analysis for absorbed energy plotted as a function of test temperature was done by a hyperbolic tangent curve fitting method to reduce errors in data interpretation. Based on the data obtained from the regression analysis, the ductile-to-brittle transition temperature (DBTT), which corresponds to the average value of upper-shelf energy (USE) and lower-shelf energy, was determined. In order to examine cleavage crack propagation path, the cross-sectional areas under the fracture surface of Charpy impact specimens fractured at 77 K (–196 °C) were observed using FE-SEM with EBSD.

III. RESULTS

A. Microstructure

All the steels used in this study showed different dual-phase microstructures composed of soft ferrite and harder low-temperature transformation phases such as granular bainite (GB), degenerate upper bainite (DUB), lower bainite (LB), and lath martensite (LM). PF is an equiaxed microstructure transformed at the highest temperatures and slowest cooling rates. As transformation temperature decreases, the low-temperature transformation phases are usually formed in the order of GB, DUB, LB, and LM.[9–11] The GB consists of equiaxed bainitic ferrites with dispersed martensite-austenite (MA) constituents and has well-developed substructure inside. The DUB is characterized by sheaves or groups of parallel bainitic ferrite laths, where MA constituents are present at the interfaces between bainitic ferrite laths unlike conventional upper bainite, while the LB contains finely dispersed carbides within bainitic ferrite laths formed from austenite grain boundaries. The LM is a highly dislocated ferrite structure formed by a diffusionless shear transformation. The microstructures of the steels investigated were differentiated in accordance with these terminologies and categories.[5,9–11] The LB/LM is regarded as a mixture of LB and LM, because it is quite difficult to distinguish them clearly without adopting TEM analysis.

Figure 3 shows SEM micrographs of the steels rolled in the single- and intercritical-phase regions. The volume fraction of PF, basic low-temperature transformation phases, and effective grain size are summarized in Table IV. The volume fraction of PF is less than 10 pct, and the grain size is smaller than 2 μm. Although the steels rolled in the single-phase region are mainly composed of DUB for major low-temperature transformation phases, the SB and SC steels contain somewhat
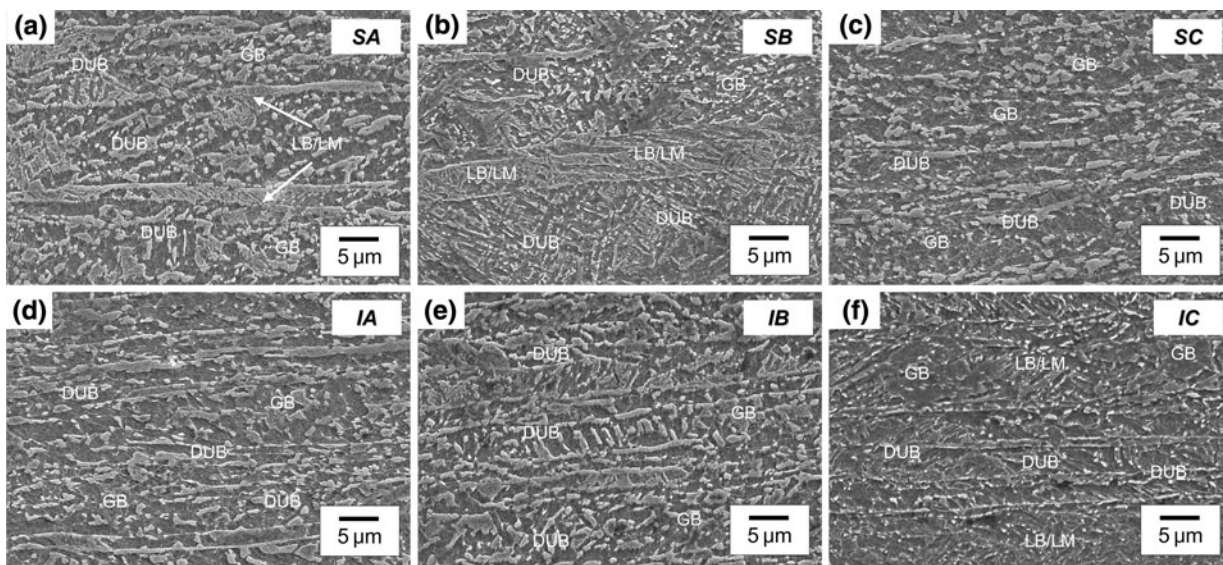

Fig. 3—SEM micrographs of the (a) SA, (b) SB, (c) SC, (d) IA, (e) IB, and (f) IC steels.

Table IV. Volume Fraction of PF, Basic Low-Temperature Transformation Phases, and Effective Grain Size

Steel	Volume Fraction of PF (Pct)	Low-Temperature Transformation Phases*		Microhardness (VHN)**	Effective Grain Size (μm)†
		Major	Minor		
SA	4.4 ± 2.6	DUB	GB, LB/LM	293 ± 10	2.2 ± 2.9
SB	2.6 ± 1.5	DUB, LB/LM	GB	335 ± 11	2.5 ± 3.6
SC	3.8 ± 2.2	DUB, GB	LB/LM	306 ± 5	3.5 ± 5.1
IA	0.9 ± 0.5	DUB, GB	LB/LM	314 ± 9	2.2 ± 3.4
IB	2.6 ± 1.6	DUB, GB	LB/LM	314 ± 12	2.1 ± 2.1
IC	7.0 ± 4.2	LB/LM, DUB, GB	—	348 ± 5	1.7 ± 2.1

*A mixture of granular bainite (GB), degenerate upper bainite (DUB), lower bainite (LB), and lath martensite (LM) transformed at low temperature.
**Measured under a 300 g load.
†Characterized by misorientations that are at least 10 deg apart.

more LB/LM and GB, respectively, than the SA steel (Figures 3(a) through (c) and Table IV). The steels rolled in the intercritical-phase region consist mostly of DUB and GB regardless of start and finish cooling temperatures. The IC steel has a considerable amount of LB/LM due to rather faster cooling rate achieved during accelerated cooling compared to the IA and IB steels (Figures 3(d) through (f), and Tables III and IV). On the other hand, the steels rolled in the single-phase region have nearly the same amount of PF, while the IC steel contains a large amount of PF where some deformed ferrites would be formed during intercritical rolling (Table IV).

The misorientation, inverse pole figure, and misorientation distribution maps of the SC and IC steels are provided in Figure 4. Grain boundaries are displayed in different colors according to the grain boundary misorientation (Figures 4(a) and (b)). In both steels, there are several isolated and equiaxed fine ferrite grains having high-angle grain boundaries of 10 deg or higher and various low-temperature transformation phases having many subgrain boundaries. The GB and DUB have many low-angle grain boundaries of 2 to 10 deg, and the LB/LM has high-angle ones of 10 deg or higher inside. The boundaries within low-temperature transformation phases or between them and ferrite, however, are mostly high-angled because they were transformed from different austenite grains (Figure 4). Furthermore, acicular ferrite (AF) plates with a chaotic arrangement facing in many different directions often appear in the IC steel, which was not mentioned in our terminology categories previously. Their formation may be attributed to rolling in the intercritical region (Figures 4(b) and (d)). It has been reported that the volume fraction of AF increases with the amount of deformation in austenite, because AF grains are formed at nucleation sites such as deformation bands, dislocations, and intragranular particles within austenite grains.[6,7,12] The IC steel with partial formation of AF showed the increased fraction of high-angle grain boundaries (Figures 4(e) and (f)). For the SC and IC steels, the effective grain size, which is characterized by misorientation of 10 deg or higher, was measured to be 3.5 and 1.7 μm, respectively (Table IV). This indicates that the

SC steel rolled in the intercritical-phase region is expected to have better low-temperature toughness than the IC steel rolled in the single-phase region because of the smaller effective grain size.

B. Tensile Properties

Room-temperature tensile stress-strain curves are presented in Figure 5 and the test results are listed in Table V. All the steels show continuous yielding behavior probably due to the presence of mobile dislocations in the ferrite.[3,4] These dislocations are by-products of the transformation from austenite to martensite or MA constituents and play a significant role in decreasing yield ratio. Since the steels investigated exhibit yield strengths exceeding 690 MPa (100 ksi) (Table V), they all satisfy the strength requirement of API X100 grade pipeline steels. The SB and IC steels show the highest yield strength above 827 MPa (120 ksi) in the steels rolled in the single- and intercritical-phase regions, respectively, presumably because of the larger amount of LB/LM. For the same cooling conditions, the yield strengths of the SA and SB steels are higher than those of the IA and IB steels, whereas the SC steel has rather lower yield strength than the IC steel.

On the other hand, the tensile strength usually increases with the volume fraction of harder low-temperature transformation phases and with the degree of their strain hardening.[3–5,13–15] The tensile strength of the SB steel is higher than that of the SA steel due to the higher volume fraction of LB/LM. Also, the SC and IC steels intermediately cooled to around 673 K (400 °C) show lower tensile strength than those cooled to room temperature because of the higher fraction of GB or PF (Figure 3, and Tables IV and V). Most of the steels investigated exhibited very low yield ratio below 0.75 and high uniform elongation above 5.0 pct, which are accepted as a typical specification suitable for strain-based applications with high deformability.[1,15]

C. Charpy Impact Properties

Figure 6 presents the Charpy energy data plotted as a function of test temperature, and the results obtained
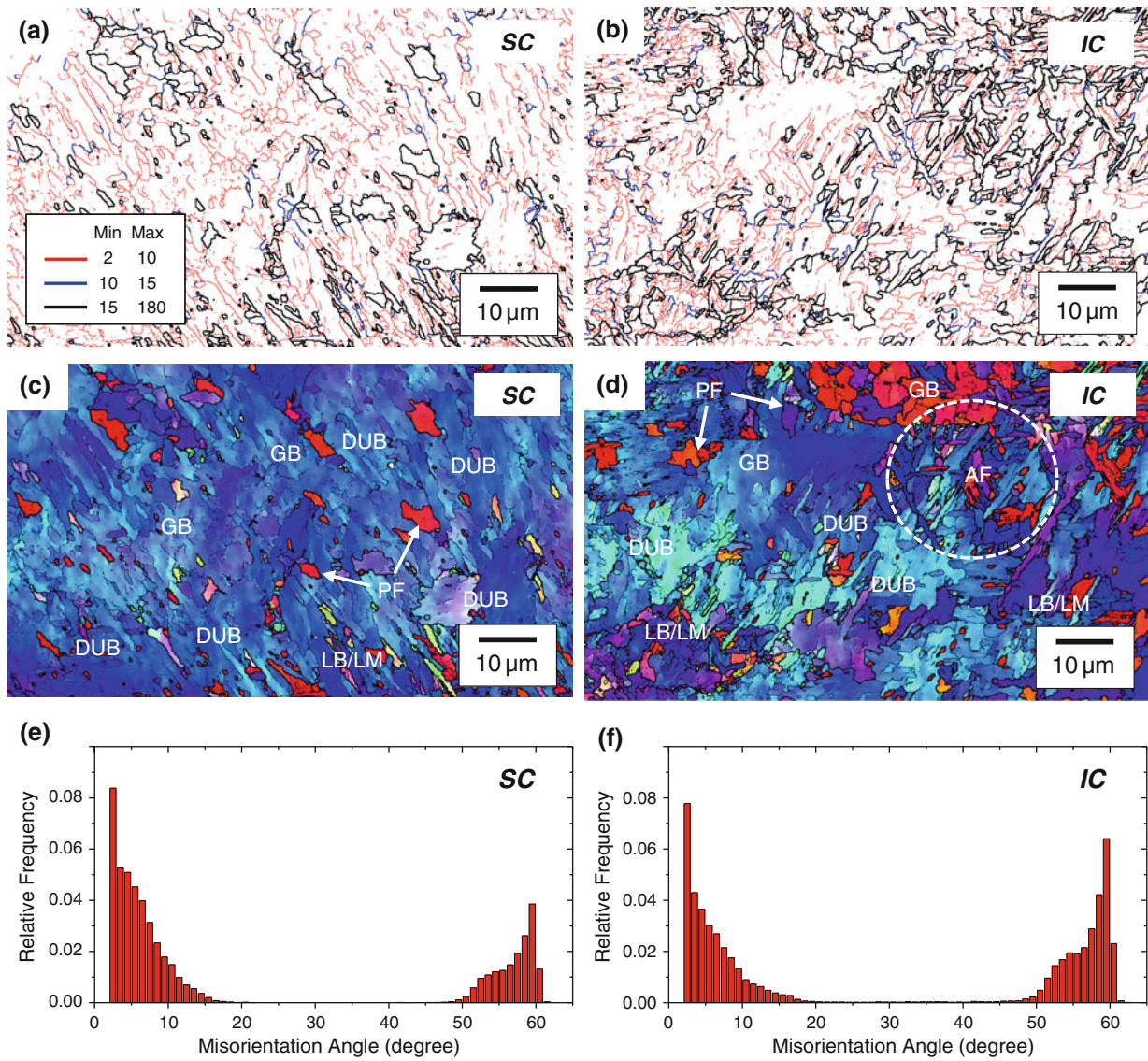
Fig. 4—(a) and (b) Misorientation, (c) and (d) inverse pole figures, and (e) and (f) misorientation distribution maps of the L-T plane of the SC and IC steels. AF grains appeared inside a white dotted circle.
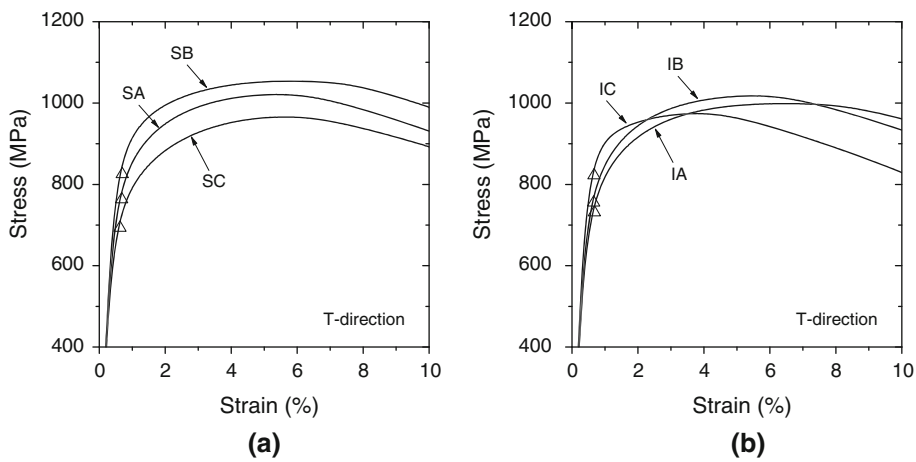

Fig. 5—Room-temperature tensile strain-stress curves of the steels cooled in the (a) single- and (b) intercritical-phase region.

Table V. Tensile and Charpy Impact Properties

| Steel | Tensile Properties | | | | Charpy Impact Properties | | |
	Yield Strength (MPa)*	Tensile Strength (MPa)*	Yield Ratio**	Uniform Elongation (Pct)**	USE (J)	Energy Absorbed at 233 K (–40 °C) (J)	DBTT K (°C)
SA	773 ± 15	1022 ± 8	0.75 ± 0.01	5.7 ± 0.3	155 ± 9	107 ± 21	219 (−54) ± 4
SB	835 ± 11	1053 ± 7	0.75 ± 0.01	5.6 ± 0.3	176 ± 23	112 ± 33	224 (−49) ± 9
SC	703 ± 6	959 ± 6	0.71 ± 0.02	7.1 ± 0.6	168 ± 12	104 ± 10	223 (−50) ± 5
IA	741 ± 3	1000 ± 3	0.71 ± 0.03	6.6 ± 0.1	104 ± 5	71 ± 10	212 (−61) ± 4
IB	765 ± 1	1020 ± 3	0.74 ± 0.03	6.5 ± 0.2	138 ± 7	108 ± 16	214 (−59) ± 4
IC	832 ± 6	982 ± 18	0.82 ± 0.03	5.8 ± 1.1	164 ± 9	138 ± 43	204 (−69) ± 5

*Transverse direction.
**Longitudinal direction.
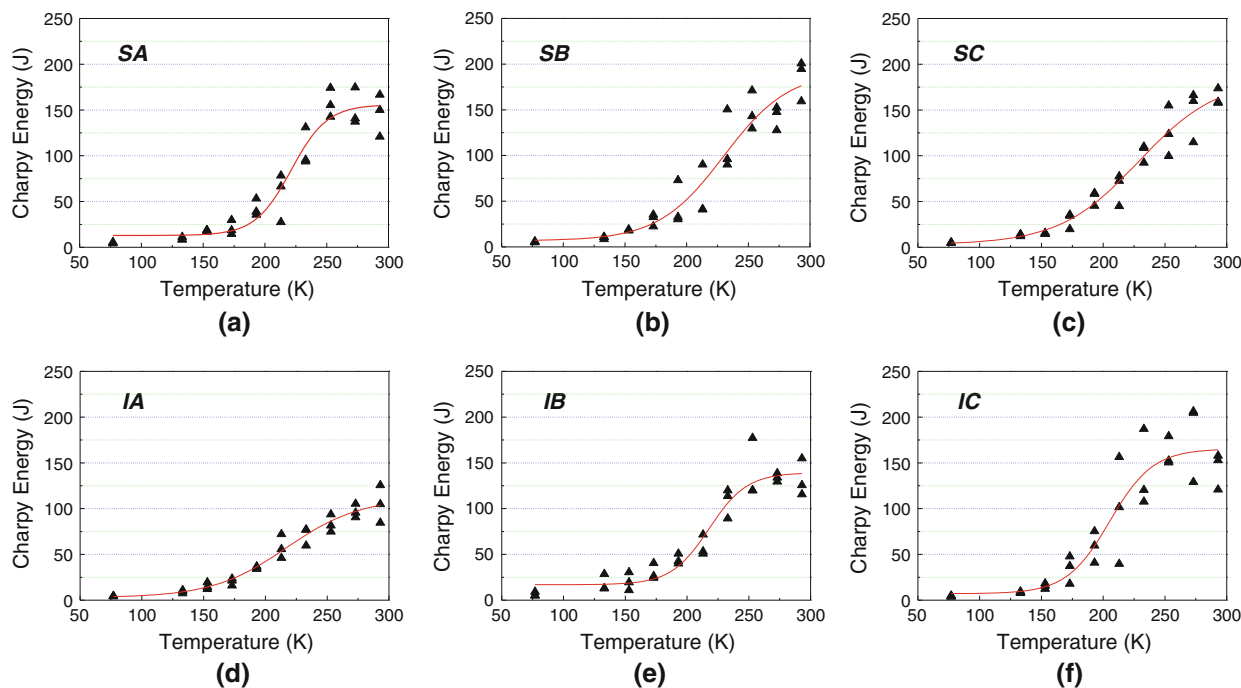
Fig. 6—Charpy impact energy plotted as a function of test temperature for the (*a*) SA, (*b*) SB, (*c*) SC, (*d*) IA, (*e*) IB, and (*f*) IC steels.

from them are given in Table V. The steels rolled in the single- and intercritical-phase regions have a USE between 130 and 180 J, and the energy absorbed at 233 K (–40 °C) usually exceeds 100 J. However, the IA steel shows inferior low-temperature toughness since the energy absorbed at 233 K (–40 °C) is 71 J due to the lowest volume fraction of ferrite. Although the steels rolled in the single-phase region have slightly higher DBTT by 283 K to 293 K (10 °C to 20 °C) than those rolled in the intercritical-phase region, on the other hand, they show little change in Charpy properties such as USE, energy absorbed at 233 K (–40 °C), and DBTT, irrespective of start and finish cooling temperatures. This is because they have nearly the same volume fraction of PF and similar low-temperature transformation phases. However, the IC steel has the highest Charpy energy absorbed at 233 K (–40 °C) (138 J) and the lowest DBTT of approximately 203 K

(–70 °C), representing the best low-temperature toughness among the steels investigated (Table V). It can be generally related to the reduction of the overall effective grain size by an appropriate formation of fine PF and various low-temperature transformation phases[12,13] (Table IV).

In order to examine the cleavage crack propagation of GB, DUB, and LB/LM structures, the Charpy specimens fractured at 77 K (–196 °C) for the SC and IC steels, which contain a large amount of GB and DUB, and LB/LM, respectively, were coated with nickel, and their cross-sectional areas beneath the fracture surface were observed by an SEM, as provided in Figure 7. Unit crack path (UCP) is commonly defined as the length of a crack in which the crack propagates almost in a straight line. According to Pickering,[16] the UCP is roughly equal to the distance between two neighboring high-angle boundaries. Many researchers have found that the
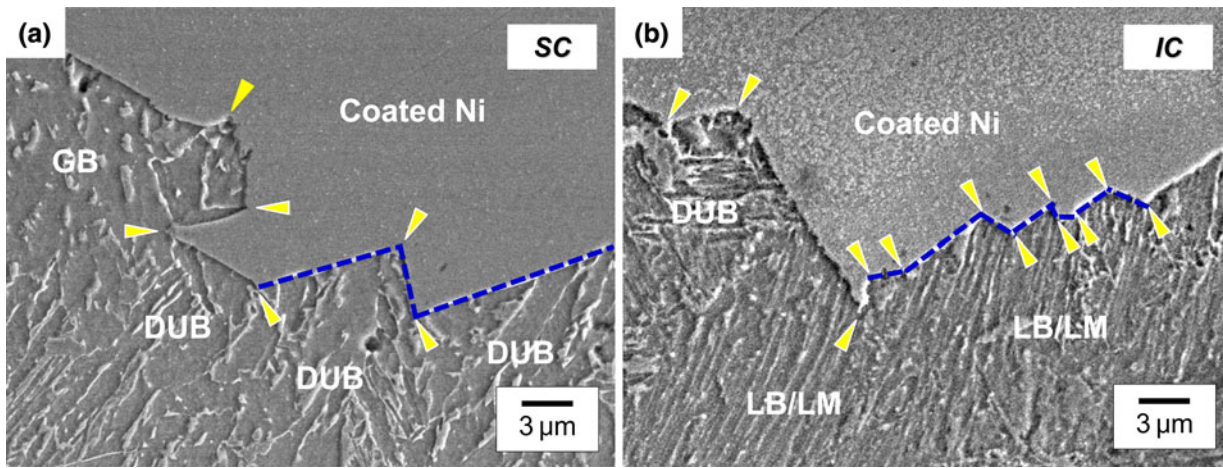
Fig. 7—SEM micrographs of the cross-sectional area beneath the cleavage fracture surface of Charpy specimens fractured at 77 K (–196 °C) for the (a) SC and (b) IC steels, showing the crack propagation path. Blue dotted lines indicate UCP.

UCP is almost the same as the ferrite grain size in ferritic steels, while it is 1.3 to 1.5 times the packet size in bainitic steels.[17,18] In steels with complex microstructures, however, it has been recognized that mean domain size characterized by crystal misorientations of at least 10 deg or more properly describes effective grain size[5,13] (Table IV). Based on the observation of the crack propagation path, it is found that the SC steel has a larger UCP than the IC steel because long crack propagation over 3 μm takes places in the SC steel consisting of GB and DUB, but the cleavage crack of the IC steel frequently changes its direction in a zigzag pattern at several LB/LM lath boundaries of the IC steel (Figure 7).

IV. DISCUSSION

The HSLA steels investigated in the present study had different dual-phase microstructures composed of soft ferrite and harder low-temperature transformation phases such as GB, DUB, LB, and LM (Figure 3 and Table IV). After the ferrite was formed from austenite during air cooling through the intercritical-phase region or during rolling in the intercritical-phase region, the various low-temperature transformation phases were developed during the subsequent accelerated cooling to ambient temperatures. The formation of PF was dependent strongly on the intercritical rolling and start cooling temperature, while the kind, size, and volume fraction of the low-temperature transformation phases were affected by the change in the transformation region and austenite hardenability resulting from carbon redistribution occurring during slow cooling through the intercritical-phase region.[6–8]

Bright-field TEM images showing PF and various low-temperature transformation phases are provided in Figures 8(a) through (c). There are several fine PF grains below 2 μm in size, and GB and DUB structures, which are characterized by granular and lath-type bainitic ferrite grains, respectively, with dispersions of martensite or MA constituent. A high density of

dislocations was also present near interfaces between ferrite and martensite or MA constituent. This is because many dislocations were formed inside ductile ferrite nearby martensite or MA constituent transformed from retained austenite by shear strain (Figure 8(c)).[4,19] These mobile dislocations contribute to lowering yield strength.[3,4] A bright-field TEM micrograph showing ferrite grains with low-density dislocation and the corresponding Kikuchi patterns confirmed that their boundaries have the nature of high-angle ones (Figures 8(d) and (e)). Figure 9(a) shows a bright-field TEM image showing fine precipitates less than 20 nm in diameter formed inside ferrite grains. According to the energy dispersion spectroscopy (EDS) spectrums, these precipitates are mostly Nb and V carbides or carbonitrides (Figure 9(b)). They can provide ferrite with additional strengthening and substantially contribute to an increase in yield strength.[5–7]

Based on the results of microstructural, EBSD, and TEM analyses, the effects of microstructure on mechanical properties and low-temperature toughening mechanisms are discussed here. Because a considerable amount of dislocations were generated inside ferrite grains in the steels rolled in the intercritical-phase region when ferrite transformed prior to intercritical rolling was deformed during intercritical rolling (Figure 8(c)), the steels rolled in the intercritical-phase region have lower USEs than those rolled in the single-phase region for the same cooling conditions.[20] In the case of energy absorbed at 233 K (–40 °C), however, the IB steel has similar energy to the steels rolled in the single-phase region and the IC steel has rather higher energy by 30 J than those (Table V) that can be related to their lower DBTT. The IC steel showed rather lower DBTT and higher low-temperature toughness than the other steels, even if its high yield strength over 830 MPa (120 ksi) may result in a loss of toughness[5–7] (Table V). The improvement in low-temperature toughness is possibly attributed to the decrease in overall effective grain size (Table IV). The toughness of dual-phase structure is primarily provided by the ferrite phase, and the DBTT and associated low-temperature toughness are affected
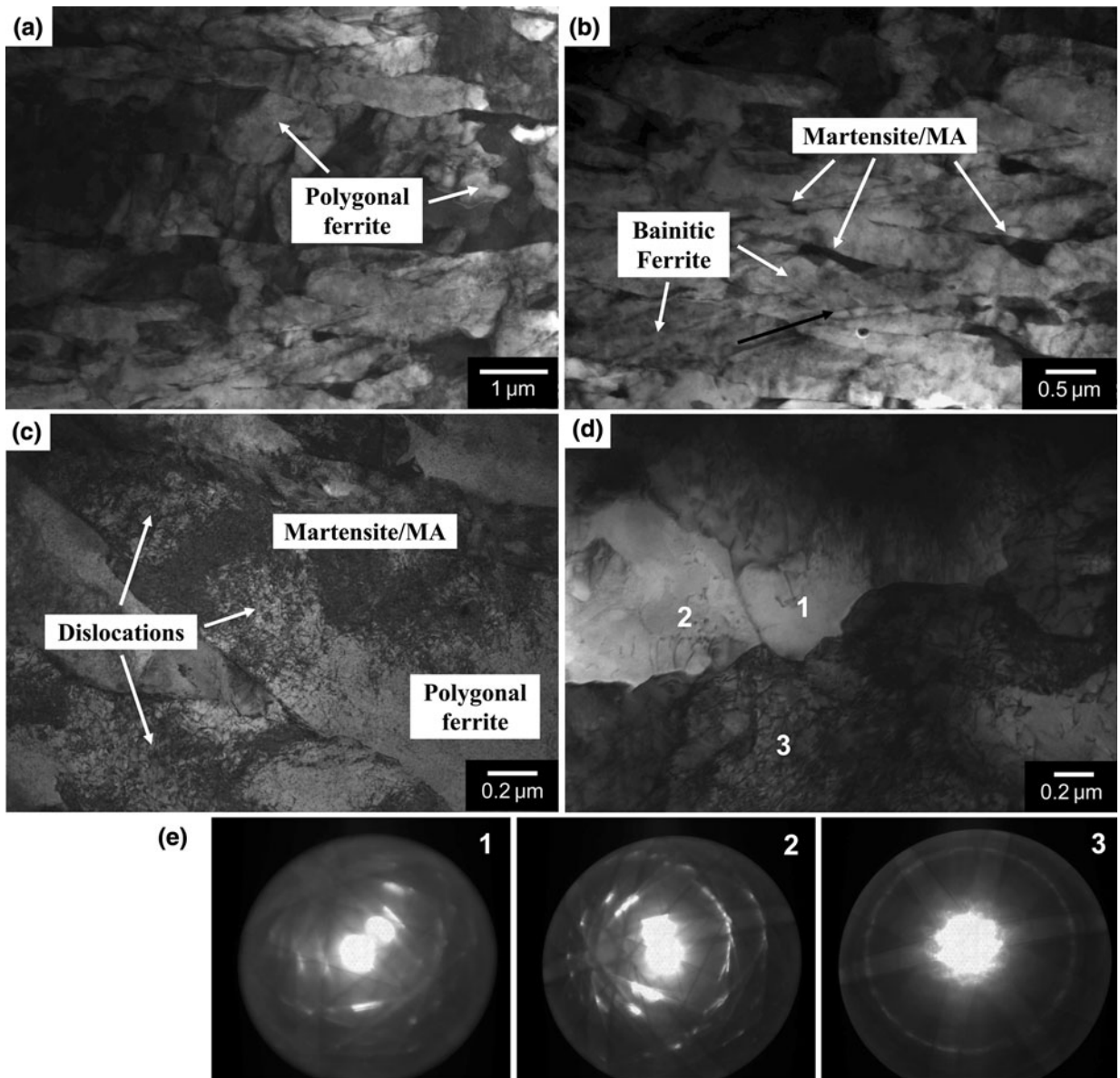
Fig. 8—TEM micrographs, showing PF, bainitic ferrite with marteniste/MA constituents, and dislocations in the IC steel: (*a*) through (*d*) bright-field TEM images and (*e*) Kikuchi patterns corresponding to (d), where grains have a common ⟨111⟩ ferrite zone axis.

by the effective grain size depending on the type, size, and volume fraction of low-temperature transformation phases as well as their intrinsic brittleness.[3–7] When many high-angled grains with large misorientation are finely formed, DBTT decreases and low-temperature toughness is enhanced by the reduction of effective grain size.[12–15,20]

Figure 10 exhibits EBSD analysis results of the cross-sectional area showing the cleavage crack propagation path of the Charpy specimen fractured at 77 K (–196 °C) for the IC steel consisting of various low-temperature transformation phases such as GB, DUB, and LB/LM. Because subgrains inside the GB have similar crystal orientations, a crack propagates long and straight during cleavage fracture (Figure 7(a)). In the DUB, the crack also proceeds linearly without changing

its direction, because its lath or block boundaries are mostly low-angle ones (Figures 4 and 7(a)). In the LB/LM, however, the crack frequently bends at high-angle block boundaries inside LB or LM, and thus, the effective grain size of the LB/LM seems to be very small (Figures 4 and 7(b)). Recent studies[21,22] on the crystallographic features of LM have reported that sub-blocks composed of two specific Kurdjumov–Sachs (K-S) variants with misorientation of about 10 deg frequently appear in ultra-low-carbon or low-carbon steels.[21,22] Furuhara *et al.*[23] also found that the effective grain size of LB was essentially smaller than that of upper bainite, because a packet of LB was divided by blocks consisting of a single variant of laths, whereas that of UB contained laths of two K-S variants with a small misorientation (sub-blocks). As with these
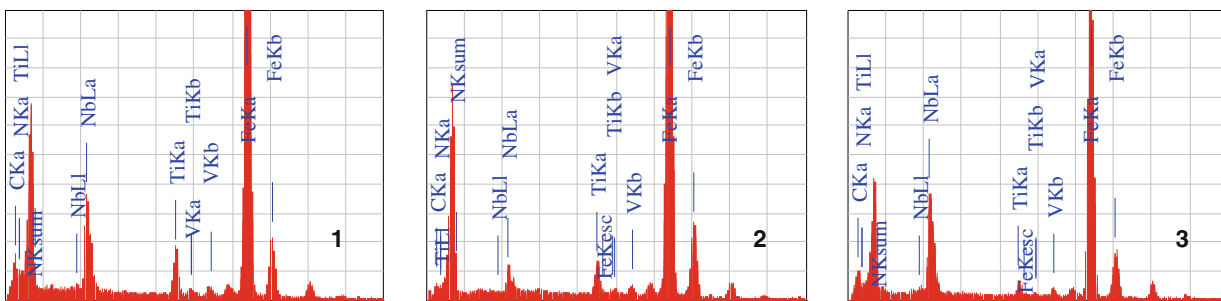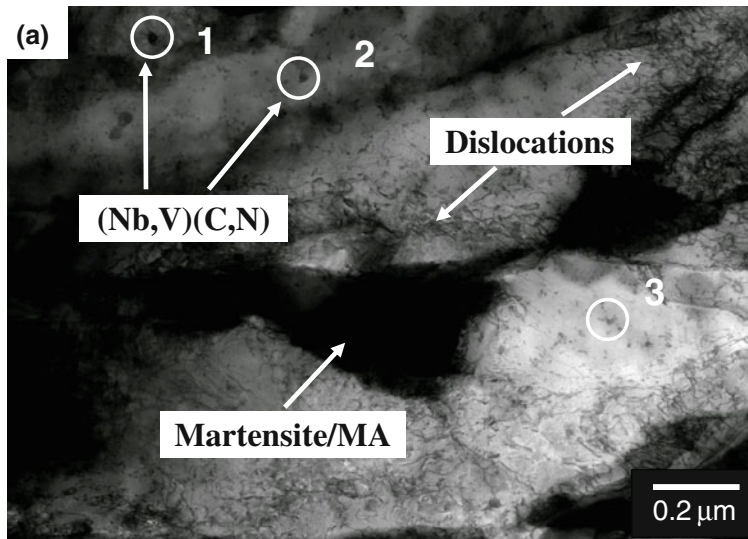
Fig. 9—TEM micrographs of the IC steel, showing the precipitation of (Nb, V)(C,N) carbide or carbonitrides inside ferrite grain: (*a*) bright-field image and (*b*) EDS spectrums corresponding to (a).
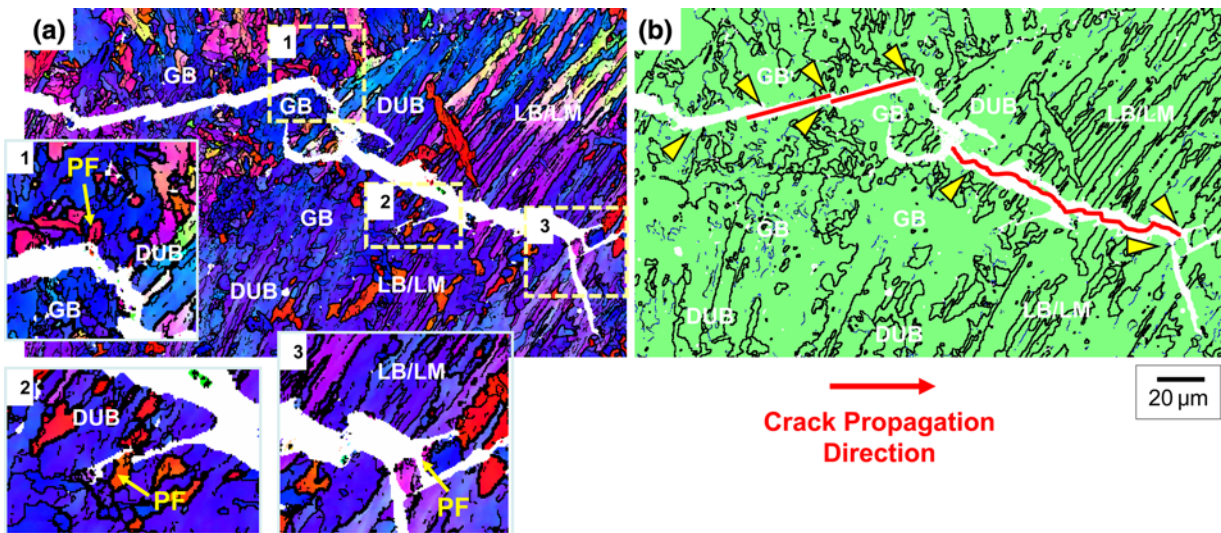

Fig. 10—EBSD analysis results of (*a*) inverse pole figure and (*b*) misorientation maps, showing cleavage crack propagation path observed under the fracture surface of the Charpy specimen fractured at 77 K (–196 °C) for the IC steel. The black lines indicate high-angle grain boundaries with misorientations larger than 15 deg.

results, it can be proposed that LB/LM has relatively small effective grain size compared to the GB and DUB (Figures 7 and 10).

Figure 11 illustrates the role of ferrite through a schematic drawing. PF already formed at the boundaries or inside low-temperature transformation phases
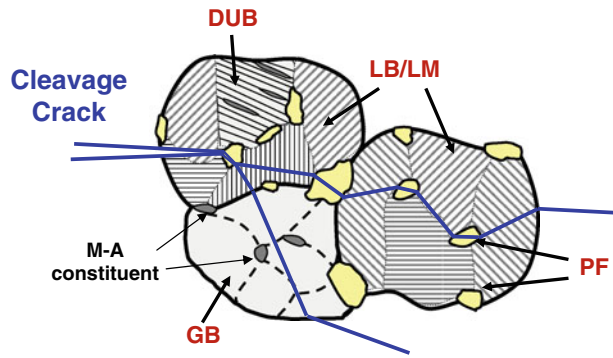
Fig. 11—Schematic illustrations of the cleavage crack propagation path in dual-phase microstructure composed of PF and various low-temperature transformation phases such as GB, DUB, and LB/LM.

interrupts and changes a crack propagation path at the boundaries between PF and low-temperature transformation phases, which is in agreement with the observation results of Figure 10. It is suggested that the incorporation of ferrite as a second phase contributes to the decrease in DBTT through the reduction of effective grain size (Figure 10(a)). Recently, Kim et al.[24] reported that the effective grain size of the AF-PF steels is similar to the distance between two adjacent PFs, because a cleavage crack changes its direction when it meets the boundaries between AF and PF. In the present study, it was observed that the boundaries between PF and low-temperature transformation phases act as beneficial barriers to cleavage crack propagation. As a result, the IC steel composed of fine PF and various low-temperature transformation phases such as GB, DUB, and LB/LM showed the best combination of high yield strength and excellent low-temperature toughness due to the frequent tortuosity of the cleavage crack propagation path by the smallest effective grain size[25] (Figures 7 and 10, and Tables IV and V).

Consequently, the low-temperature toughening mechanism could be explained by the decrease in overall effective grain size that results from the presence of fine PF and a mixture of various low-temperature transformation phases such as GB, DUB, and LB/LM. These findings indicate that dual-phase microstructures should be composed of fine PF and various low-temperature transformation phases through a precise design of chemistry and thermomechanical processing conditions, which involve the refinement of prior austenite grains by increasing rolling reduction ratio in a nonrecrystallization region and controlling accelerated cooling conditions. In the present study, HSLA steels having high yield strength and excellent low-temperature toughness with good deformability were successfully fabricated by varying intercritical rolling, start, and finish cooling temperatures. To develop HSLA steels with a better combination of high strength and low-temperature toughness, and enhanced deformability in the future, therefore, clearer understanding of crystallographic microstructural factors and of quantitative correlation between them and mechanical properties will be a prerequisite.

V. CONCLUSIONS

In the present study, HSLA steels were fabricated by varying thermomechanical processing conditions such as rolling and cooling conditions in the intercritical region, and the low-temperature toughening mechanism was investigated in terms of microstructure and associated grain boundary characteristics.

1. HSLA steels with different dual-phase microstructures consisting of fine PF and various low-temperature transformation phases such as GB, DUB, and LB/LM showed good combinations of high strength and low-temperature toughness as well as excellent deformability of low yield ratio below 0.75 and high uniform elongation above 5.0 pct by the adjustment of thermomechanical processing conditions composed of rolling in the intercritical region and subsequent cooling.
2. The steels acceleratedly cooled to higher temperature had lower tensile strength than those cooled to room temperature due to the increased volume fraction of granular bainite or PF irrespective of rolling in the intercritical region, while the yield strength varied with intercritical rolling and start and finish cooling temperatures that affect the formation of PF and various low-temperature transformation phases.
3. For the same start and finish cooling temperatures, the steels rolled in the intercritical-phase region had slightly lower USE since a relatively large amount of dislocations was generated during the intercritical rolling, but had better low-temperature toughness due to their lower DBTT than those rolled in the intercritical-phase region. The steels rolled in the single-phase region showed little change in Charpy impact properties, because they have nearly the same volume fraction of PF and similar low-temperature transformation phases despite different cooling conditions.
4. According to the SEM and EBSD analysis results, the low-temperature toughness could be greatly improved by the reduction of overall effective grain size because fine PFs are frequently present and a mixture of LB and LM acts as obstacles effectively preventing cleavage crack propagation. As a result, the steel rolled in the intercritical-phase region and cooled to approximately 673 K (400 °C) provided the best combination of high yield strength and excellent low-temperature toughness due to the smallest effective grain size and the appropriate formation of low-temperature transformation phases.

REFERENCES

1. D.B. Lillig, B.D. Newbury, and S.A. Altstadt: *Proc. 19th Int. Offshore and Polar Eng. Conf*, ISOPE, Osaka, Japan, 2009, pp. 1–10.
2. Y. Mizutani, K. Ishibashi, K. Yoshii, Y. Watanabe, R. Chijiwa, and Y. Yoshida: *Nippon Steel Techn. Rep.*, 2004, vol. 90, pp. 45–52.
3. A.T. Davenport: *Formable HSLA and Dual Phase Steels*, AIME, New York, NY, 1979.
4. N.J. Kim and G. Thomas: *Metall. Trans. A*, 1981, vol. 12A, pp. 483–89.
5. J. Koo, M.J. Luton, N.V. Bangaru, R.A. Petkovic, D.P. Fairchild, C.W. Petersen, H. Asahi, T. Hara, Y. Terada, M. Sugiyama, H. Tamehiro, Y. Komizo, S. Okaguchi, M. Hamada, A. Yamamoto, and I. Takeuchi: *Int. J. Offshore Polar Eng.*, 2004, vol. 14, pp. 2–10.
6. I. Tamura, H. Sekine, T. Tanaka, and C. Ouchi: *Thermomechanical Processing of High-Strength Low-Alloy Steels*, Butterworth & Co. Ltd, London, 1988.
7. T. Gladman: *The Physical Metallurgy of Microalloyed Steels*, The Institute of Materials, London, 1997.
8. US Patent Pub. No. 20070193666.
9. B.L. Bramfitt and J.G. Speer: *Metall. Trans. A*, 1990, vol. 21A, pp. 817–29.
10. G. Krauss and S.W. Thompson: *ISIJ Int.*, 1995, vol. 35, pp. 937–45.
11. T. Hayashi, F. Kawabata, and K. Amano: *Proc. Materials Solution '97 on Accelerated Cooling/Direct Quenching Steels*, ASM, Materials Park, OH, 1997, pp. 93–99.
12. Y.M. Kim, H. Lee, and N.J. Kim: *Mater. Sci. Eng. A*, 2008, vol. 478, pp. 361–70.
13. B. Hwang, Y.G. Kim, S. Lee, Y.M. Kim, N.J. Kim, and J.Y. Yoo: *Metall. Mater. Trans. A*, 2005, vol. 36A, pp. 2107–14.
14. P.-H. Chang and A.G. Preban: *Acta Metall.*, 1985, vol. 33, pp. 897–903.
15. V. Schwinn, P. Fluess, A. Liessem, and J. Schroeder: *Proc. 18th Int. Offshore and Polar Eng. Conf*, ISOPE, Vancouver, Canada, 2008, pp. 27–32.
16. F.B. Pickering: *Proc. Symp. on Transformation and Hardenability in Steels*, Climax Molybdenum Co., Ann Arbor, MI, 1967, pp. 109–29.
17. P. Brozzo, G. Buzzichelli, A. Mascanzoni, and M. Mirabile: *Met. Sci.*, 1977, vol. 11, pp. 123–29.
18. Y. Ohmori, H. Ohtani, and T. Kunitake: *Met. Sci.*, 1974, vol. 8, pp. 357–66.
19. J.H. Chen, Y. Kikuta, T. Araki, M. Yoneda, and Y. Matsuda: *Acta Metall.*, 1984, vol. 32, pp. 1779–88.
20. B. Hwang, S. Lee, Y.M. Kim, N.J. Kim, and J.Y. Yoo: *Metall. Mater. Trans. A*, 2005, vol. 36A, pp. 1793–1805.
21. H. Kitahara, R. Ueji, N. Tsuji, and Y. Minamino: *Acta Mater.*, 2006, vol. 54, pp. 1279–88.
22. S. Morito, X, Huang, T. Furuhara, T. Maki, and N. Hansen: *Acta Mater.*, 2006, vol. 54, pp. 5323–31.
23. T. Furuhara, S. Morito, and T. Maki: *Proc. 1st Int. Symp. on Steel Science*, ISIJ, Kyoto, Japan, 2007, pp. 51–56.
24. Y.M. Kim, S.K. Kim, Y.J. Lim, and N.J. Kim: *ISIJ Int.*, 2002, vol. 42, pp. 1571–77.
25. B. Hwang, Y.M. Kim, S. Lee, N.J. Kim, and S.S. Ahn: *Metall. Mater. Trans. A*, 2005, vol. 36A, pp. 725–39.